World Academy of Science, Engineering and Technology
International Journal of Geological and Environmental Engineering
Vol:10, No:2, 2016

Sand Production Modelled with Darcy Fluid Flow Using Discrete Element Method

M. N. Nwodo, Y. P. Cheng, N. H. Minh

***Abstract*—**In the process of recovering oil in weak sandstone formations, the strength of sandstones around the wellbore is weakened due to the increase of effective stress/load from the completion activities around the cavity. The weakened and de-bonded sandstone may be eroded away by the produced fluid, which is termed sand production. It is one of the major trending subjects in the petroleum industry because of its significant negative impacts, as well as some observed positive impacts. For efficient sand management therefore, there has been need for a reliable study tool to understand the mechanism of sanding. One method of studying sand production is the use of the widely recognized Discrete Element Method (DEM), Particle Flow Code (PFC^{3D}) which represents sands as granular individual elements bonded together at contact points. However, there is limited knowledge of the particle-scale behavior of the weak sandstone, and the parameters that affect sanding. This paper aims to investigate the reliability of using PFC^{3D} and a simple Darcy flow in understanding the sand production behavior of a weak sandstone. An isotropic tri-axial test on a weak oil sandstone sample was first simulated at a confining stress of 1MPa to calibrate and validate the parallel bond models of PFC^{3D} using a 10m height and 10m diameter solid cylindrical model. The effect of the confining stress on the number of bonds failure was studied using this cylindrical model. With the calibrated data and sample material properties obtained from the tri-axial test, simulations without and with fluid flow were carried out to check on the effect of Darcy flow on bonds failure using the same model geometry. The fluid flow network comprised of every four particles connected with tetrahedral flow pipes with a central pore or flow domain. Parametric studies included the effects of confining stress, and fluid pressure; as well as validating flow rate – permeability relationship to verify Darcy's fluid flow law. The effect of model size scaling on sanding was also investigated using 4m height, 2m diameter model. The parallel bond model successfully calibrated the sample's strength of 4.4MPa, showing a sharp peak strength before strain-softening, similar to the behavior of real cemented sandstones. There seems to be an exponential increasing relationship for the bigger model, but a curvilinear shape for the smaller model. The presence of the Darcy flow induced tensile forces and increased the number of broken bonds. For the parametric studies, flow rate has a linear relationship with permeability at constant pressure head. The higher the fluid flow pressure, the higher the number of broken bonds/sanding. The DEM PFC^{3D} is a promising tool to studying the micromechanical behavior of cemented sandstones.

***Keywords*—**Discrete Element Method, fluid flow, parametric study, sand production/bonds failure.

M. N. Nwodo was with the Department of Civil, Environmental, and Geomatics Engineering, University College London (UCL), UK (e-mail: martin42007@yahoo.com).

Y. P. Cheng is with the Department of Civil, Environmental, and Geomatics Engineering, UCL, UK (e-mail: yi.cheng@ucl.ac.uk).

N. H. Minh was with UCL, and is now with the School of Engineering, Nazarbayev University, 53 Kabanbay Batyr Avenue, Astana 010000, Kazakhstan (e-mail: minh.nguyen@nu.edu.kz).

I. Introduction

THIS research seeks to validate the reliability of using Discrete Element Method, DEM Particle Flow Code, PFC to study the behavior of weak oil sandstones, and applies hydrodynamic forces to check on the effect of fluid flow on sanding. A significant proportion of the world's oil reserves is found in weakly-consolidated sandstone reservoirs which are liable to sand production [1]. In a study [2], it was stated that about 70% of the world's oil reserves are contained in weakly-consolidated reservoirs while [3] estimated that 60% of all petroleum reservoirs in the world are sandstones.

It was observed [2] that during production of hydrocarbons from a weak sandstone oil reservoir and under special circumstances, sand particles move from the reservoir into the well along with the hydrocarbon flow, the quantity of which varying from a few grams per cubic meter of reservoir fluid to catastrophic level, possibly leading to complete filling of the borehole and eventually the loss of the well.

Some of the other problems of uncontrolled sand production, depending on the severity, include: wellbore instability, collapse of some parts of a horizontal well in unconsolidated formations, environmental surface pollution, additional cost of remedial and clean-up operations, and pipelines and surface facilities erosion [1].

Complicating the matter, sanding, triggered by fluid flow, was also found to boost primary oil production and prevents skin damage of wellbore [4] while the installation of conservative measures for sand control may lead to lower productivity. There is need to balancing the cost-effectiveness of conventional sand control measures employed in the field (e.g., gravel packs and filters).

Several models (experimental, analytical, and numerical) and failure criteria (mostly hydromechanical and shear) have been used to study sand production mechanism. According to a review by [1], numerical models are by far the most powerful tools for predicting sanding in weak formations; can be combined with analytical correlations to obtain more efficient results, and calibrated or validated using experimental results for use in analyzing oil field problems. The commonly used numerical model for studying sand production is the DEM which better represents sands as distinct granular particles cemented together, as opposed to continuum numerical approaches.

The commercial DEM code PFC^{3D} has been mainly used to study sand production. However, there is limited knowledge of the particle-scale behavior of weak sandstone, and that of the parameters that affect sanding. This paper aims to investigate the reliability of using PFC^{3D} 3.0 in understanding

the behavior of compacted oil weak sandstone; effects of confining stress, and fluid flow pressure; as well as validating flow rates and permeability relations, with regards to bond failure/sanding.

II. Literature Review

A. Sand Production Causes and Criteria

Sand production or sanding is a phenomenon that occurs in the oil and gas industry during the extrusion of hydrocarbon [5]. It is worth noting here that the model in this paper will be considering horizontal oil well (see Fig. 1), where the axial and radial stresses in sample represent the horizontal and vertical stresses in the field respectively.

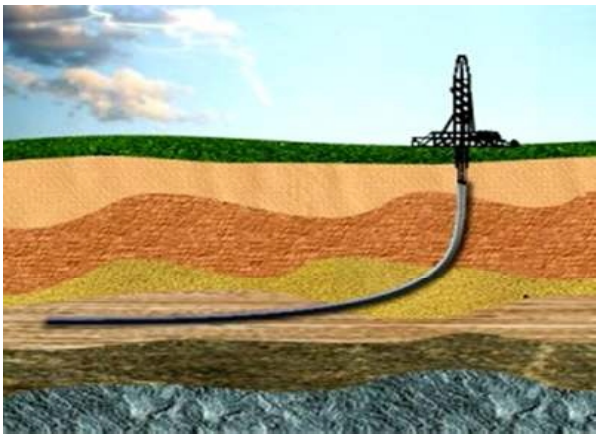

Fig. 1 Illustrating horizontal oil well drilling

Originally, before drilling, weak sandstone formation is in hydromechanical equilibrium, meaning that the in-situ stresses and pore pressure are in static equilibrium [2]. During drilling of well bores, formations around the hole undergo shear failure, the radius of the shear-failed zone being inversely proportional to the strength properties of the formation [6]. This idea of shear failure causation is in agreement with the research [7] showing that sand production (see Fig. 2) can be triggered either by compressive (shear) failure induced by the near cavity pore pressure gradient. Hence, the inquisition into the criteria for sand production prediction: whether compression (shear) failure or tensile failure or any other criteria.

According to [7], sanding criteria used in sand production models mainly include: shear and tensile failure criteria, a critical pressure gradient criterion, a criterion of critical plastic deformation, and erosion based criteria. Reference [8] in their study summarized the sanding criteria into three: shear failure, cohesive tensile failure, and Equivalent Plastic Strain (EPS) failure which agrees with [9]. Bond failure due to both compression and shear were considered in this paper.

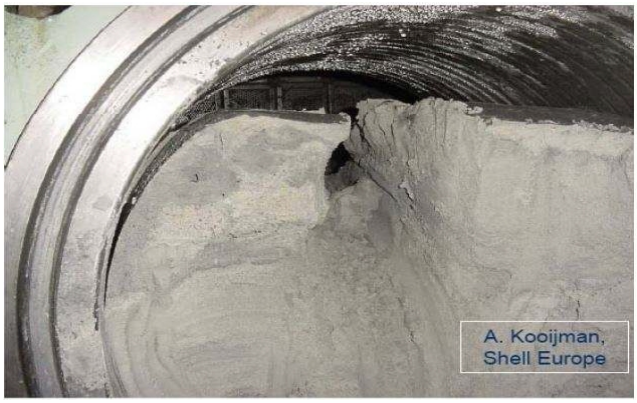

Fig. 2 Sand production at North Sea field [20]

B. Effect of Fluid Flow on Sanding

Reference [8] seems not to have considered the effect of fluid flow on the mechanisms of sanding. A recent research on sand production, coupling DEM with Computational Fluid Dynamics, CFD, [10] reveal that erosion of formation particles due to fluid flow is an important feature of sanding problems. The study is in agreement with [11] who used coupled DEM and CFD to simulate the rate of sanding with fluid flow at different flow velocities, shown in Fig. 3.

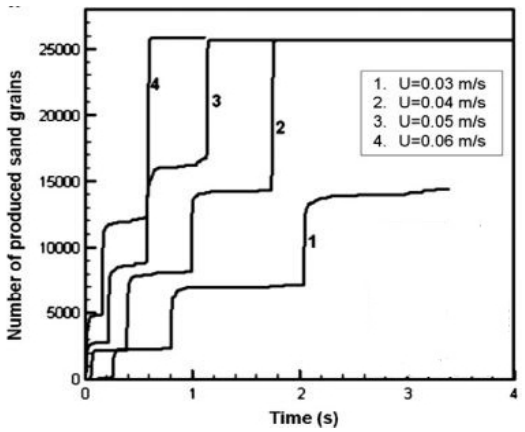

Fig. 3 Rate of sanding with fluid flow at various flow velocities [11]

While another recent study [12] agrees that fluid drag force initiates sanding; it, however, maintains that inter-granular bonds are the most important factor in preventing sand production. The effect of simple Darcy fluid flow on particle bonds failure was applied in this paper.

C. Review on Sanding Prediction Models

There have been researches on a wide range of models for predicting sand production. Details on the models can be found in [1]. The DEM, first introduced by [13] and thoroughly described in [14], [15], can be used to simulate, in a dynamic manner, the disintegration of granular media subjected to loading, with each particle of the granular media considered as an individual entity with a geometric representation of its surface topology and a description of its physical state.

Several researchers have studied sand production using two

dimensional (2D) PFC^{2D} DEM code [16]-[19]. The 2D models provide an understanding of the fundamental physics involved in sand production and the importance of fluid properties in sanding. Reference [18] simulated hollow cylinder tests of circular disks superimposed with a fluid flow mesh in 2D to study sanding and found three failure patterns similar to those observed in laboratory experiments.

Reference [17] showed that the number of broken bonds in numerical models has a close relationship with the strength of the sample (see Fig. 4). In their work introducing fluid flow networks, [17] also argued that DEM model may not result in realistic macroscopic friction coefficients if only circular or spherical grain shapes are used. But [18] overcame this limitation by setting the bond strength so high that no bonds in the model will fail due to inherent stress in the bond. Instead, all bonds associated with a given disk only break when the stresses inside the disk satisfy a failure criterion composed of tensile, shear, and compressive failure.

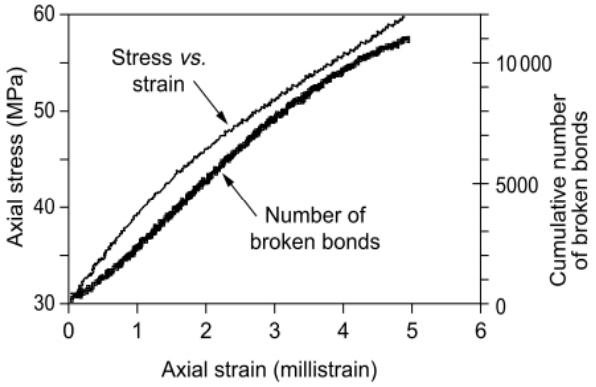

Fig. 4 Relationship between number of broken bonds and strength of sample [17]

There is limited knowledge of the particle-scale behavior of weak sandstone, and that of the parameters that affect sanding. This paper aims at investigating the reliability of using PFC^{3D} in understanding the behavior of compacted oil weak sandstone, effects of confining stress, fluid flow pressure, flow rate, and permeability on bonds failure/sanding.

III. Methodology

A. Sample Preparation

A series of computer simulations were performed using DEM commercial code, PFC^{3D} 3.0. The general procedure is shown on work flow chart – Fig. 5.

Isotropic tri-axial tests were first simulated at a confining stress of 1MPa to calibrate and validate the parallel bond models of the DEM PFC^{3D} code. The weak oil sandstone sample used was adapted from the experimental work of [2]. The model geometry used was cylindrical with 10m, 10m height and diameter respectively, shown on Fig. 7. The particles or spherical balls were generated at random and packed irregularly to represent a granular material with an internal unordered structure. Boundary stresses were calculated by summing the reaction forces on boundary wall and dividing by the wall area. As a check for initial equilibrium, the ratio of maximum unbalanced force to the maximum contact force was ensured to be less than 0.01 after particles generation.

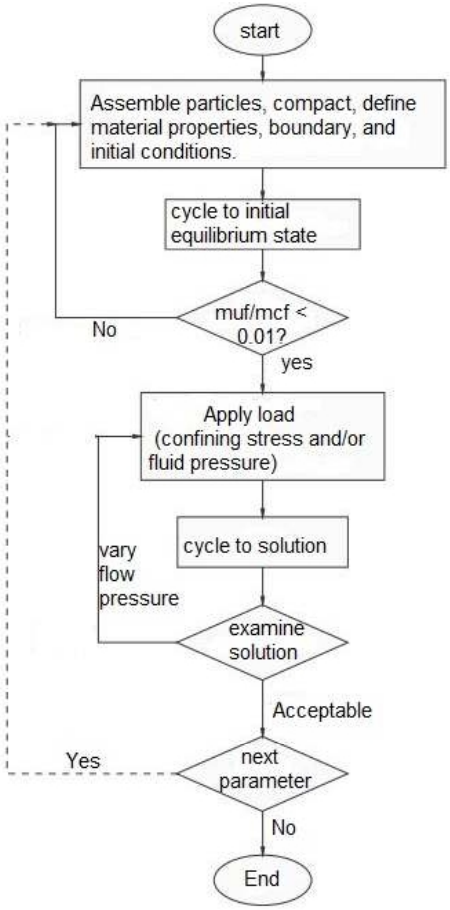

Fig. 5 General work flow chart for methodology

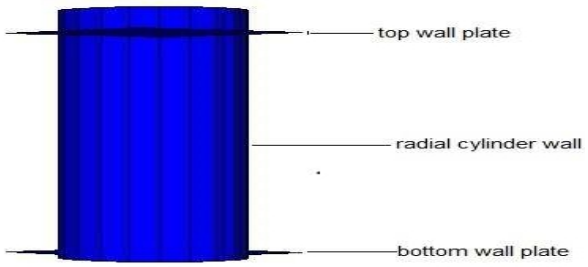

Fig. 6 Radial cylindrical wall with top and bottom wall plates

Three boundary frictionless walls were first made: one cylindrical wall, and two wall plates at the top and bottom (see Fig. 6). Since it was not possible to apply forces directly to walls because the equation of motion is not solved for walls in PFC, the velocities of the walls were controlled by a numerical servo-mechanism to achieve a specified confining reaction forces, hence, stress.

The porosity was 0.30, the particle size was 0.4m. The number of sandstone particles or balls generated was 2050. The input parameters included particle stiffness of 1GN/m,

parallel bond parameters of 30MPa bond strength, 13GN/m parallel bond stiffness, and 69.5% parallel bond radius by interparticle bond volume. The density of the particles was set to 2650kg/m^3, the initial particle friction coefficient was set low to 0.1 during packing and compaction, in accordance with literature, in order to achieve the target porosity. The actual friction coefficient was set to 0.6494 (33 degrees) during the failure test. A summary of the input parameters for the UCS test is shown on Table I.

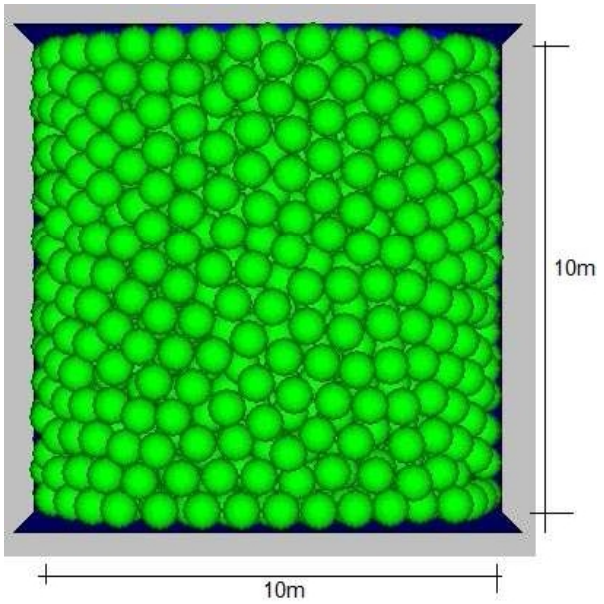

Fig. 7 Cylindrical model with spherical balls

The desired isotropic axial and radial stress was 1MPa. The walls were extended by a factor of 0.1 to allow for large straining to occur during the test. The walls stiffness before compaction was set to 1GN/m; but after initial compaction, the cylindrical wall stiffness was reduced to one-tenth (0.1GN/m) of the particles stiffness in order to simulate a "soft" confinement. The strains in the radial and axial directions were computed using the general relation:

$$\varepsilon = \frac{(Lo-L)}{0.5*(Lo+L)} \quad (1)$$

where **ε** is the strain in radial or axial direction, **Lo** is the original radius or sample length, and **L** is the new radius or sample length. The sample was then loaded to failure by releasing the top and bottom platens from servo control and increasing their velocities in a controlled manner. The output data included the confining stress, deviator stress, axial strain, and volumetric strain.

B. Formation of Flow Network

The fluid flow network comprised of domains of pores created by every four neighboring particles (see Fig. 8) such that each flow link or pipe was a face of a tetrahedron. As a result of the limitation of PFC^{3D} 3.0 to only axial flow (radial flow was not applicable), the boundary values for the flow pressure could only be set at the top and bottom walls of the model. The initial top boundary flow pressure was set to zero while the initial bottom flow pressure was set to 0.8MPa. A steady state pressure condition was observed after cycling to solution. The flow rate obeyed Darcy's flow law, stated in (2):

$$q = \frac{k*a^3*\Delta Pp}{L'} \quad (2)$$

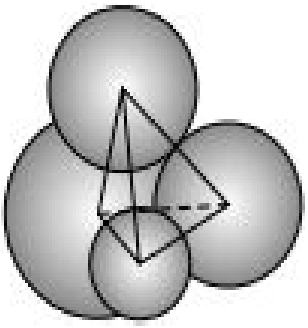

Fig. 8 A fluid flow network [17]

TABLE I
INPUT PARAMETERS FOR ISOTROPIC TRIAXIAL TEST

Input Parameter	Value	Unit
Normal / shear particle stiffness	1.0	GN/m
Friction coefficient	0.6494	
Porosity	0.3	
Particle size	0.4	m
Density of particles	2650	kg/m^3
Normal / shear parallel bond strength	30	MPa
Normal and shear parallel bond stiffness	13	GN/m
Parallel bond radius	69.5	%
Number of particles	2050	
Axial / radial stress	1	MPa

In (2), **q** is the flow rate in m^3/s, **k** is the conductivity or permeability, **a** is the flow aperture or pore within a domain which varied depending on the normal contact force (if compressive) and particle separation distance (if tensile), **ΔPp** is the difference in flow pressure perturbations in force per area, and **L'** is the mean distance between the centers of the subjected domain and adjacent domains.

The response pressure due to initial pressure perturbation is given as:

$$\Delta \Pr = \frac{Kf*q*\Delta t}{Vd} \quad (3)$$

where **Kf** is the unit fluid bulk modulus set to 1GPa, **Vd** is the apparent volume of the domain, and **Δt** is time step set to 0.1 as a trial solution of (2):

$$\Delta t = \frac{L'*Vd}{N*Kf*k*a\hat{}3} \quad (4)$$

where **N** is the maximum number of pipe given as 21916. The force vector impacted on a typical particle due to the flow was calculated as:

$$Fi = P * ni * A \quad (5)$$

where **P** is the uniform pressure difference 0.8MPa, **ni** is a unit vector, **A** is a projective area on the particle determined by the contacting points with the other neighboring particles.

In attempt to verify Darcy's law at laminar fluid flow, arbitrary values of the coefficients of permeability were chosen, ranging from 0.25 to 1.0 (see Table II). The flow rate was then calculated from (2). The flow aperture, **a** = 0.1823m, was outputted after cycling to solution. The applied fluid flow pressure was constant at 0.8MPa. The graph of flow rate against permeability was plotted in Fig. 9, showing a linear relationship.

It is worth noting here that all the fluid flow pressures applied in the course of this research were axial, and not radial. The reason is that PFC^{3D} 3.0 used in the research is limited to only axial fluid flow.

IV. Results and Discussions

A. Uniaxial Compression Tests

In this section, the results from the computer simulations are presented, and interpreted. Using the same model geometry, and corresponding input parameters, simulations were conducted with and without fluid flow. Similar procedure as the isotropic tri-axial test for UCS was performed except the following: that the walls velocities were not increased to cause compressive failure. The results from the isotropic tri-axial tests are shown in Figs. 10-12.

A steep slope with clear peak strength of the sample, in Fig. 10, can be deduced. Data successfully calibrated the 4.4MPa UCS of the chosen sample gotten from Fig. 10 using the formula: $UCS = (\sigma d/2 + \sigma 3) * 0.6494$ where **σd** is deviator stress, **σ3** is confining stress, 0.6494 is the friction coefficient. The steep slope is probably due to the additional stiffness of parallel bonding. The observed shape in stress-strain graph (Fig. 10) is similar to stress-strain behavior of 4.5% cementation of drained sample reported in [21] while the peak normalized stress of around 0.85 (Fig. 11) is similar to [22].

TABLE II
Flow Rate – Permeability Study

Permeability (Darcy)	Flow rate (m^3/s)
0.25	4039
0.50	8078
0.75	12117
1.00	16156

In Fig. 12, volume-strain graph indicates initial contraction followed by dilation behavior, typical of sands behavior.

Model size scale factor was checked by also running the isotropic tri-axial test with 4m height, 2m diameter model. At parallel bond radius of 100% by bond volume, being the only adjusting parameter, the same UCS was obtained.

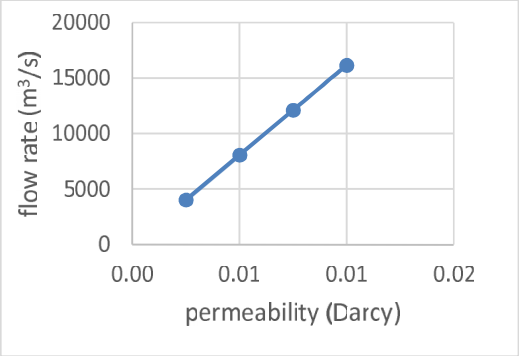

Fig. 9 Flow rate against permeability to verify simple Darcy's fluid flow law

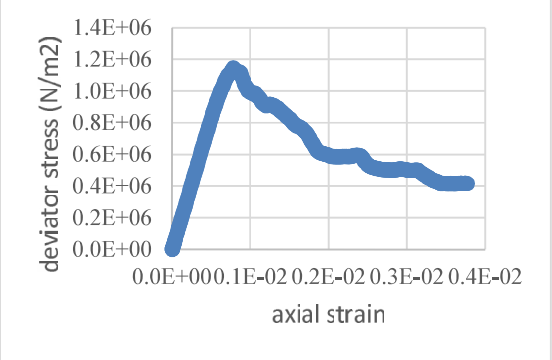

Fig. 10 Stress-strain relationship for determination of UCS of the sample

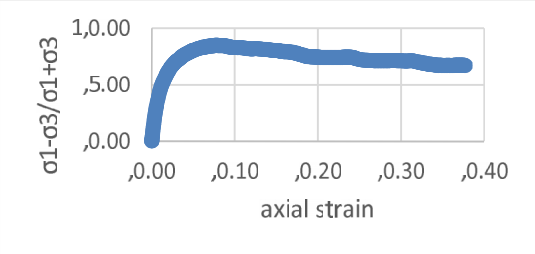

Fig. 11 Normalized stress-strain behavior to further validate the stress-strain relationship of sample. σ1 and σ3 are major and minor effective principal stresses respectively

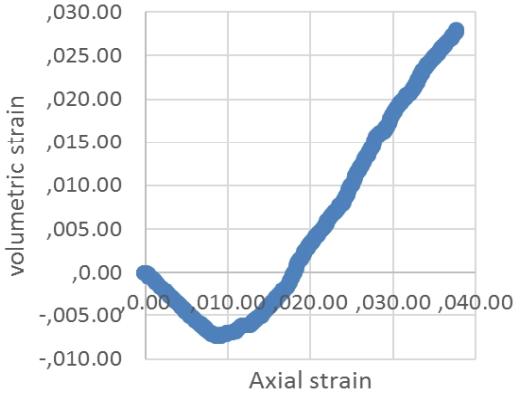

Fig. 12 Volume and axial strain behavior showing contraction and dilation observable mainly in sands

B. Tests without Fluid Flow

Without fluid flow, two simulations, checking on the effect of the presence of only confining stress on the number of broken bonds, were performed using confining stresses of 1.8MPa and 10.8MPa to serve as lower and upper stress boundaries of the sample's UCS.

The results from the simulations without fluid flow at 1.8MPa and 10.8MPa effective stresses both indicated zero number of broken bonds.

Ten simulations were conducted without fluid flow at confining stresses ranging 0.5MPa to 2.5MPa (see Table III). During each of the simulations, 30% by diameter of the sample cylindrical model was made hollow from the center, just after particles compaction and assembly. This was achieved by deleting the particles/balls within the required central region. Then, as a result of the applied external boundary confining stress, de-bonded balls would be forced towards the hollow region. These balls would be deleted after cycling to solution, and termed sanding. Figs. 15 and 16 show the graphs of confining stress against number of sanding.

C. Tests with Fluid Flow

With fluid flow, two simulations were performed but with fluid pressure considered; one at 1MPa effective confining stress, 0.8MPa fluid pressure; the other at 10MPa effective confining stress, 0.8MPa fluid pressure. Input parameters are shown in Table IV. These two simulations were to evaluate the effects of fluid flow and confining stress on sanding. The fluid considered was benzene with a permeability of approximately 1.0 Darcy, bulk modulus of approximately 1GPa. The number of the broken bonds recorded was 1175 particle bonds, regardless of the applied confining stress.

TABLE III
SANDING – CONFINING STRESS STUDY

Confining stress (MPa)	Sanding
0	0
0.5	197
0.8	195
1.0	191
1.2	187
1.4	181
1.6	197
1.8	182
2.0	174
2.2	180
2.5	175

Then, parametric studies were conducted on confining stresses, and fluid pressure, as well as establishing the flow rate-permeability relationship in attempt to verify Darcy's fluid flow law. To check on the effects of changes in fluid pressure on sanding, four simulations were conducted at fluid flow pressures of 0.4MPa to 1.0MPa (see Table V) at constant confining stress of 1MPa. At each simulation, after cycling to solution, the total number of broken bonds was recorded, and is shown in Fig. 13. In the presence of fluid flow, the number of broken bonds increased significantly with fluid pressure, which confirmed the tensile action of fluid flow reported in [10]. This also confirms the similar relationship between the number of broken bonds and sample strength investigated by [17]. However, the density of broken bonds increased with the application of the hydrodynamic pressure as opposed to the findings of [10] who employed radial hydrostatic pressure.

TABLE IV
INPUT PARAMETERS RELATED TO TESTS WITH FLUID FLOW

Fluid flow parameters	Values	Units
Confining stress	1 / 10	MPa
Fluid flow pressure	0.8	MPa
Bulk modulus	1	GPa
Length of flow pipe	0.3	m
Permeability	1	Darcy

TABLE V
VARIATIONS OF FLUID PRESSURE (MPA)

0,4
0,6
0,8
1,0

The time history of the bonds breakage was outputted for each simulation, and is shown in Fig. 14, it shows a similar stepping trend to [11] in Fig. 3.

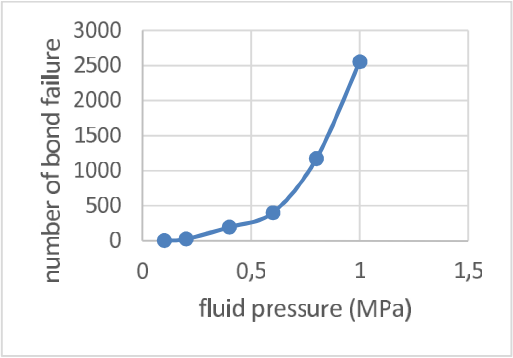

Fig. 13 Number of bond failure against fluid pressure

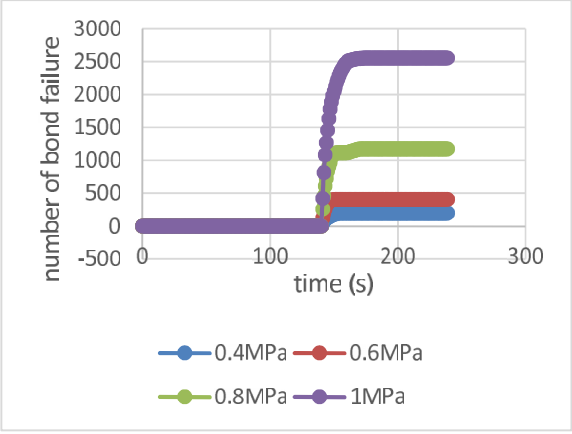

Fig. 14 Time histories of bond failures at various fluid pressures

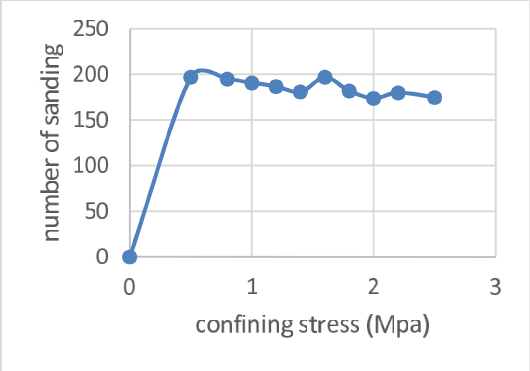

Fig. 15 Number of produced sands with confining stress for 10m height, 10m diameter model size

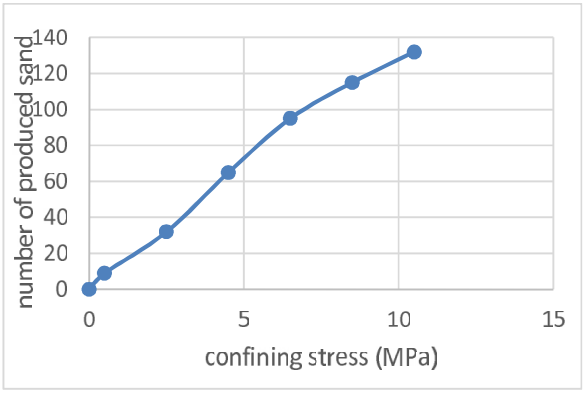

Fig. 16 Relationship of number of produced sands with confining stress using 4m height, 2m diameter model size, showing model scale effect.

Finally, a result showing the major effect of model size scaling is shown in Fig. 16. It was noted the effect of model size scaling on the observable results. The most evident and reported on this paper is the sanding-confining stress relationship. With the model size of 10m height and 10m diameter used throughout the paper, there seems to be an exponential increasing relationship (Fig. 15) between number of sanding and applied confining stress. However, when reducing the model size to 4m height and 2m diameter, a curvilinear relationship (Fig. 16) was obtained between the numbers of sanding and applied confining stress. This implies that sample model scaling seems important while using PFC in studying the sanding behavior of weak sandstones, though, often neglected by researchers using the numerical tool.

V. Conclusion

By successfully calibrating the parallel bond model for a weak sandstone sample, the PFC numerical tool seems reliable in studying the micromechanical behavior of weak oil sandstones. Establishing this confidence at the use of the tool will enable a faster and more economical means of predicting the sanding behavior of weak sandstones in sandstones reservoir, with the view to properly manage and control sanding for efficient oil production in such oil reservoirs.

With the observed stiff, sharp peak strength, and strain softening, the parallel bond model seems to depict the behavior of real cemented sandstones. The presence of hydrodynamic fluid flow induces tensile force in the particle-fluid interaction, and may contribute to tensile failure of particles within the cavity region during oil production. As a further study, a better understanding of the micromechanical behavior of real weak sandstones is required, including investigations on the effect of particle crushing on sand production.

Acknowledgment

M. N. Nwodo thanks Dr. Y. P. Cheng and Dr. N. H. Minh for their comments and guidance throughout the research and writing up of this paper.

References

[1] H. Rahmati, *et al.*, "Review of sand production prediction models," *Journal of Petroleum Engineering,* vol. 2013, article ID 864981, pp. 1-17, Nov. 2012.

[2] V. Fattahpour, M. Moosavi, and M. Mehranpour, "An experimental investigation on the effect of rock strength and perforation size on sand production," *Journal of Petroleum Science and Engineering,* vol. 2012, no. 86-87, pp. 172-189, Mar. 2012.

[3] K. Bjorlykke, *Petroleum Geoscience: from Sedimentary Environments to Rock Physics.* Berlin: Springer, 2010.

[4] H. H. Vaziri, E. Lemoine, I. D. Palmer, J. McLennan, and R. Islam, "How can sand production yield a several-fold increase in productivity: experimental and field data," at *SPE Annu. Technical Conf. and Exhibition,* Texas, 2000, pp. 1-4.

[5] P. G. Ranjith, M. S. A. Perera, W. K. G. Perera, S. K. Choi, and E. Yasar, "Sand production during the extrusion of hydrocarbons from geological formations: a review," *Journal of Petroleum Science and Engineering,* vol. 124, pp. 72-82, Oct. 2014.

[6] H. H. Vaziri, E. M. Lemoine, and Y. Xiao, "Quantification of sand production induced improvement in productivity index," *Canadian Geotechnical J.,* vol. 39, pp. 1088-1102, Sept. 2002.

[7] A. Nouri, H. Vaziri, E. Kuru, and R. Islam, "A comparison of two sanding criteria in physical and numerical modelling of sand production," *Journal of Petroleum Science and Engineering,* vol. 2006, no. 50, pp. 55-70, Oct. 2005.

[8] Y. Wang, and E. Papamichos, "Sand prediction by different criteria and validation through a hollow cylinder test," at *the 46th U.S. Rock Mechanics/Geomechanics Symposium,* Chicago, 2012, pp. 24-27.

[9] Y. H. Wang, and S. C. Leung, "A particulate-scale investigation of cemented sand behavior," *Canadian Geotechnical J.,* vol. 45, pp. 29-44, Feb. 2008.

[10] N. Climent, M. Arroyo, C. O'Sullivan, and A. Gens, "Sand production simulation coupling DEM with CFD," *European Journal of Environmental and Civil Engineering,* vol. 18, no. 9, pp. 983-1008, May, 2014.

[11] Z. Y. Zhou, A. B. Yu, and S. K. Choi, "Numerical simulation of the liquid-induced erosion in a weakly bonded sand assembly," *Powder Technology,* vol. 211, pp. 237-249, Apr. 2011.

[12] B. Ikporo, and O. Sylvester, "Effect of sand invasion on oil well production: a case study of Garon field in the Niger Delta," *The International Journal of Engineering and Science,* vol. 4, no. 5, pp. 64-72, 2015.

[13] P. A. Cundall, "A computer model for simulating progressive large scale movement in blocky rock systems," in *Proceedings of the Symposium of International Society of Rock Mechanics,* France, vol. 1, paper no. II-8, 1971.

[14] P. A. Cundall, "Formulation of a three-dimensional distinct element model – Part I. A scheme to detect and represent contacts in a system composed of many polyhedral blocks," *International Journal of Rock Mechanics, Mineral Science and Geomechanics,* vol. 25, no. 3, pp. 107-116, 1988.

[15] R. Hart, P. A. Cundall, and J. Lemos, "Formulation of a three-dimensional distinct element model – Part II. Mechanical calculations for motion and interaction of a system composed of many polyhedral

blocks," *International Journal of Rock Mechanics, Mineral Science and Geomechanics,* vol. 25, no. 3, pp. 117-125, 1988.
[16] R. M. O'Connor, J. R. Torczynski, D. S. Preece, J. T. Klosek, and J. R. Williams, "Discrete element modelling of sand production," *International Journal of Rock Mechanics and Mining Sciences,* vol. 34, no. 231, pp. 3-4, 1997.
[17] L. Li, and R. M. Holt, "Particle scale reservoir mechanics," *Oil and Gas Science and Technology,* vol. 57, no. 5, pp. 525-538, 2002.
[18] L. Li, E. Papamichos, and P. Cerasi, "Investigation of sand production mechanisms using DEM with fluid flow," *Multiphysics Coupling and Long Term Behavior in Rock Mechanics,* London, 2006.
[19] D. O. Potyondy, "Simulating stress corrosion with a bonded-particle model for rock," *International Journal of Rock Mechanics and Mining Sciences,* vol. 44, pp. 677-691, 2006.
[20] E. Papamichos, "Sand production physical and experimental evidence," at the *French 18th ALERT School-Geomechanical and Structural Issues in Energy Production, Aussois, 2006.*
[21] S. M. Haeri, A. Seiphoori, and A. Rahmati, "The behavior of a limy cemented gravely sand under static loading-case study of Tehran alluvium," *Electronic Journal of Geotechnical Engineering,* vol. 13, pp. 1-10, 2008.
[22] L. Y. G. Cheung, C. O'Sullivan, and M. R. Coop, "Discrete element method simulations of analogue reservoir sandstones," *International Journal of Rock Mechanics and Mining Sciences,* vol. 63, pp. 93-103, July, 2013.